



# Electrodeposited Ag catalysts for the electrochemical reduction of CO<sub>2</sub> to CO



Yu Seok Ham<sup>a</sup>, Seunghoe Choe<sup>a</sup>, Myung Jun Kim<sup>a</sup>, Taeho Lim<sup>b</sup>, Soo-Kil Kim<sup>c,\*</sup>,  
Jae Jeong Kim<sup>a, \*\*</sup>

<sup>a</sup> School of Chemical and Biological Engineering, Institute of Chemical Process, Seoul National University, 1 Gwanak-ro, Gwanak-gu, 08826, Seoul, South Korea

<sup>b</sup> Department of Chemical Engineering, Soongsil University, 369 Sangdo-ro, Dongjak-gu, 06978, Seoul, South Korea

<sup>c</sup> School of Integrative Engineering, Chung-Ang University, 84 Heukseok-ro, Dongjak-gu, 06974, Seoul, South Korea

## ARTICLE INFO

### Article history:

Received 10 August 2016

Received in revised form 21 January 2017

Accepted 10 February 2017

Available online 14 February 2017

### Keywords:

CO<sub>2</sub> electrochemical reduction

Electrocatalyst

Ag

Dendrite

Ethylenediamine

## ABSTRACT

For the electrochemical reduction of CO<sub>2</sub> to CO, a dendrite-type Ag catalyst was fabricated via an electrodeposition method in an ammonia-based Ag deposition solution containing ethylenediamine (EN) as an additive. The influence of electrodeposition parameters on the properties of this catalyst was examined and further correlated with CO production efficiency. The addition of EN changed the intensity ratio of (220) vs. (111) planes in the Ag catalyst, which was shown to be proportional to the CO production activity. Furthermore, EN modified the chemical shift of Ag3d<sub>5/2</sub> in the negative direction, increasing the CO production efficiency. Under optimized deposition conditions (~0.45 V vs. Ag/AgCl, 40 mM EN), which were a compromise between intensity ratio and chemical shift, the fabricated Ag catalysts exhibited the highest Faradaic efficiency and mass activity for CO during CO<sub>2</sub> electrolysis in 0.5 M KHCO<sub>3</sub>. The experimental correlation between CO production efficiency and the crystalline/electronic structures of the catalyst suggested guidelines for further improving the Ag catalyst activity.

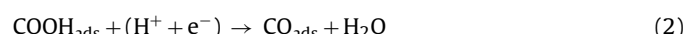
© 2017 Elsevier B.V. All rights reserved.

## 1. Introduction

Electrochemical reduction of CO<sub>2</sub> is regarded as a promising technology for mitigating the greenhouse effect [1–8], aiming to convert CO<sub>2</sub> into valuable carbon products, such as CO, HCOOH, CH<sub>4</sub>, or CH<sub>3</sub>OH, using electrical energy from clean and renewable energy sources. Among these carbon products, CO has received the great attention due to its use in syngas (a mixture of CO and H<sub>2</sub>), which is an intermediate resource for the production of methanol, ammonia, and synthetic hydrocarbon fuels via the Fischer–Tropsch process [9]. To date, Au, Ag, Zn, Pd, and Ga have been shown to efficiently catalyze the selective conversion of CO<sub>2</sub> to CO [8,10–14]. Ag has received particular attention owing to its excellent catalytic activity and moderate price. Therefore, the synthesis and characterization of Ag catalysts have been investigated intensively [12,15–20].

According to recent theoretical and simulation studies [21,22], various reaction intermediates on the catalyst surface are involved

in CO production. The reduction of CO<sub>2</sub> to CO is known to involve electrochemical and thermochemical reactions, as described in Eqs. 1–3 [22].



In addition to reactions 1–3, the hydrogen evolution reaction (HER) simultaneously occurs on the cathode surface, as presented by Eqs. 4 and 5 [22]. Since HER reduces the Faradaic efficiency (FE) of CO production, it must be considered in catalyst design.



CO production efficiency could be improved by either promoting the reactions related to Eqs. 1–3 or inhibiting HER (Eqs. 4 and 5). The binding energies of COOH<sub>ads</sub> and CO<sub>ads</sub> are important, particularly for Eqs. 1–3, and they are strongly affected by the crystallographic orientation of the catalyst surface, as reported by Back et al. using density functional theory (DFT) calculations [22]. They showed that the Ag (110) facet provided the strongest

\* Corresponding author. Tel.: +82 28205770; Fax: +82 28138159.

\*\* Corresponding author. Tel: +82 2 880 8863, Fax: +82 2 888 1604.

E-mail addresses: [sookilkim@cau.ac.kr](mailto:sookilkim@cau.ac.kr) (S.-K. Kim), [jjkimm@snu.ac.kr](mailto:jjkimm@snu.ac.kr) (J.J. Kim).

binding with  $\text{COOH}_{\text{ads}}$  among the low-index surfaces (Ag (111), Ag (100), and Ag (110)), while the binding energies of  $\text{H}_{\text{ads}}$  on those planes were almost constant, indicating that the Ag (110) plane was the most efficient catalytic plane for the reduction of  $\text{CO}_2$  among low-index surfaces. Additionally, Hoshi et al., using single crystals fabricated by the Bridgman method, also showed that the Ag (110) plane led to a higher CO partial current than Ag (111) and Ag (100) [23]. Both theoretical and experimental studies have demonstrated the importance of controlling the crystalline planes of the catalyst to improve the activity. These reports by Back and Hoshi gave us important inspiration, but they are still only strongly supported by a few studies. In addition, to generalize the results from single crystal catalysts, we need to investigate catalysts fabricated by conventional methods, such as impregnation, precipitation, mixing, and electrodeposition, which normally afford polycrystalline structures with micro-to-nanometer dimensions. More importantly, the easy control of crystallographic structures during catalyst synthesis to produce the desired facets is necessary from a practical standpoint.

Electrodeposition is one of the most efficient ways to fabricate catalysts for various applications [13,24–33]. Usually, organic additives are used to control the various physicochemical properties of the deposit, such as morphology, electrical properties, and crystallinity [34–38]. One notable advantage of this method is its feasibility when modifying properties related to the catalytic activity, achieved by simply controlling the electrolyte composition and applied potential [32,39,40]. In particular, for Ag electrodeposition, amine-containing additives are capable of changing the crystallographic orientation of the Ag film [41,42], although the detailed mechanism was not clear. Using  $\text{NH}_3$  in  $\text{NO}_3$ -based electrolytes appeared to increase the intensity of the Ag (200) and Ag (220) planes and decrease the average crystalline size [41]. In contrast, using polyethylenimine (PEI) in an  $\text{NH}_3$ -based electrolyte significantly suppressed the development of the Ag (200) plane [42]. These studies showed that proper use of an amine-containing additive led to modification of the surface orientation, resulting in improved catalytic activity.

For this reason, an electrodeposition method using organic additives is used in this study to investigate the relationship between the crystallographic structures of Ag catalysts and the CO production efficiency, and also to facilitate the production of the desired catalysts. We fabricated a dendrite-type Ag catalyst for the reduction of  $\text{CO}_2$  to CO using electrodeposition with ethylenediamine (EN) as an additive. The variables for Ag electrodeposition, such as deposition potential, EN concentration, and deposition amount, were investigated, and the resulting facet developments, in combination with the electronic structures, were correlated with CO production efficiency. This simultaneously suggests a guide for the easy fabrication of high-activity Ag catalysts for CO production.

## 2. Experimental

### 2.1. Electrode preparation

Ag electrodeposition was conducted using a potentiostat (EG&G 2273, Princeton Applied Research). Ag-displacement deposited Cu foil, a platinum mesh, and Ag/AgCl (satd. KCl) were used as working, counter, and reference electrodes, respectively. Ag displacement on Cu foil was preliminarily performed for 30 s in electrolyte composed of silver nitrate ( $\text{AgNO}_3$ ; 99.9%, Kojima), ammonium sulfate ( $(\text{NH}_4)_2\text{SO}_4$ ; 99%, Daejung), and ammonia solution ( $\text{NH}_4\text{OH}$ ; 25.0~28.0%, Daejung). This is to prevent unwanted and uncontrolled displacement of Ag on the Cu foil during direct electrodeposition of Ag on Cu, and to minimize the exposure of substrate Cu to prevent the formation of by-products by Cu during  $\text{CO}_2$  conversion. Prior to Ag displacement, Cu foil was immersed for

2 min in an etching solution containing 0.03 M citric acid ( $\text{C}_6\text{H}_8\text{O}_7$ ; 99.5%, Daejung) and 0.034 M potassium hydroxide (KOH; 85%, Daejung) to remove native Cu oxide, and then washed with deionized water [43,44]. The electrolyte for Ag electrodeposition was the same as that for Ag displacement, except for the amounts of the components and the addition of designated amounts of EN ( $\text{C}_2\text{H}_8\text{N}_2$ ; 99%, Aldrich); each electrolyte composition is shown in Table 1. The Ag electrodeposition potential was selected by linear sweep voltammetry (LSV) analysis on a Ag rotating disk electrode (RDE) with a 50 mV/s scan rate at 300 rpm. From these results, deposition was performed at potentials of  $-0.45$ ,  $-0.8$ , and  $-1.2$  V (vs. Ag/AgCl) with charge amounts of  $1 \text{ C}/\text{cm}^2$ . The resulting Ag deposits were carefully rinsed with deionized water and dried with  $\text{N}_2$  gas.

### 2.2. Material characterization

Surface morphology, crystallinity, surface electronic state, and mass of electrodeposited Ag dendrite were characterized using field emission scanning electron microscopy (FE-SEM; S-4800, Hitachi), transmission electron microscopy (TEM; JEM-2100F, JEOL Ltd.), X-ray diffraction (XRD; D8-Advance, BRUKER), X-ray photoemission spectroscopy (XPS; SIGMA PROBE, Thermo Fisher Scientific), and inductively coupled plasma atomic emission spectroscopy (ICP-AES; Shimadzu, JP/ICPS-7500).

### 2.3. Electrochemical characterization and $\text{CO}_2$ reduction

The roughness factor (RF) of the Ag catalysts was measured using LSV analysis in a  $\text{N}_2$ -purged 0.1 M KOH solution. The potential was swept from  $-1.5$  to  $0.6$  V (vs. Ag/AgCl) at a 50 mV/s scan rate. The prepared Ag dendrite catalysts were oxidized by LSV to form a monolayer of  $\text{AgOH}$  or  $\text{Ag}_2\text{O}$  [12,45]. The RF values were calculated using the charge amounts for monolayer oxidation.

Using the prepared Ag dendrite catalysts,  $\text{CO}_2$  electrolysis was performed using a potentiostat (EG&G, 263A, Princeton Applied Research) in an H-type cell divided into cathodic and anodic parts by an NRE-212 membrane separator.  $\text{CO}_2$ -saturated 0.5 M  $\text{KHCO}_3$  and 0.5 M KCl solutions were used as catholyte and anolyte, respectively.  $\text{CO}_2$  purging was performed to the catholyte at a flow rate of 10 mL/min during electrolysis. The purging rate was carefully controlled and monitored using the mass flow controller (F-201C-FAC-22-V, Bronkhorst) and mass flow meter (F-111B-200-AAD-22V, Bronkhorst), respectively. Electrodeposited Ag catalysts, platinum gauze, and a saturated calomel electrode (SCE) were used as the working, counter, and reference electrodes, respectively. The reduction potential of  $\text{CO}_2$  was fixed at  $-1.5$  V (vs. SCE), where FE of CO was maximized in our previous  $\text{CO}_2$  electrolysis experiment [30]. The gases produced were transferred directly into a gas chromatography (GC, HP 5890, Hewlett-Packard) system, using He carrier gas, to measure the concentrations of CO and  $\text{H}_2$ . The FE was evaluated based on the concentrations of CO and  $\text{H}_2$  measured by GC and the total charge consumed during electrolysis [46].

## 3. Results and discussion

To determine the deposition potential of Ag, LSV analysis was conducted on Ag RDE with various EN concentrations in the electrolytes, as shown in Fig. 1. As the potential swept from OCP in the negative direction, the following reactions occurred sequentially at the resulting points of inflection in the i-V curves: Ag ion reduction, nitrate ion reduction, and HER. Details of each reaction and respective reduction potentials can be found in the literature [42,47,48].

It should be noted that in the presence of EN, the onset potential for Ag reduction shifted negatively from 0.42 V (AgEN0) to 0.19 V (AgEN40) and then 0.07 V (AgEN400), all vs. Ag/AgCl, accompanying

**Table 1**  
Composition of prepared solutions.

Component	Displacement solution	AgENO	AgEN20	AgEN40	AgEN100	AgEN400
AgNO <sub>3</sub> (mM)	59	10	10	10	10	10
NH <sub>4</sub> OH (M)	3.47	0	0	0	0	0
EN (mM)	0	0	20	40	100	400
(NH <sub>4</sub> ) <sub>2</sub> SO <sub>4</sub> (M)	0.58	0.6	0.6	0.6	0.6	0.6

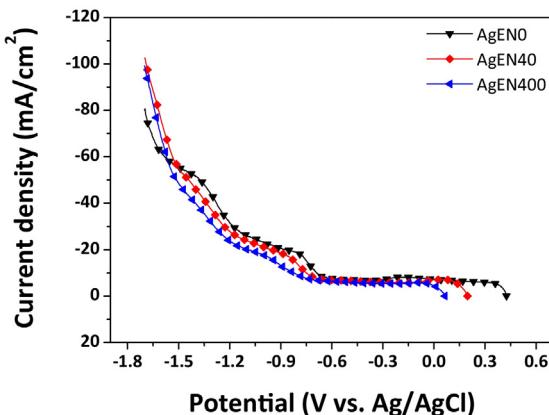


Fig. 1. LSV results on Ag RDE for the various electrolytes.

a decrease in the Ag reduction current. This behavior was consistent with other amine-containing additives such as PEI, EDTA, and NH<sub>3</sub> [34,35,41,42,49]. From the LSV results, the deposition potentials were selected using two criteria. First, the potentials had to be negative enough to induce the mass transfer limitation leading to dendrite shape deposits with large surface areas. Second, side reactions such as nitrate reduction should be minimized. Therefore, a potential of -0.45 V vs. Ag/AgCl were selected as the deposition potential, while -0.8 and -1.2 V were also tested to compare the effect of deposition potential on Ag catalyst properties.

The morphologies of pristine Cu foil and Ag deposits after galvanic displacement and electrodeposition at -0.45, -0.8, and -1.2 V vs. Ag/AgCl are presented in Fig. 2(a)–(h). After displacement (Fig. 2(b)), Ag clusters with lateral diameters of 50–500 nm formed on the Cu foil. Subsequent electrodeposition resulted in dendritic Ag deposits, while the dimension of the dendritic branches was a function of the deposition potential. Regardless of whether EN was present (c, e, g: in the absence of EN; d, f, h: in the presence of EN), the size of dendritic branches gradually decreased with increasing deposition potential. This tendency was related to enhanced nucleation under a high negative deposition potential and the severe mass transport limitation of Ag ions at the electrode surface, which subsequently led to the appearance of new dendrites rather than the growth of existing dendrites. Consequently, in this case, the dendrite size was reduced. Notably, the presence of EN increased the size of dendrite branches somewhat at the given deposition potentials, which was probably due to the slight shift in deposition reaction from severe mass transport limitation to the direction of charge transport limitation through inhibition of the deposition kinetics by added EN, as indicated in Fig. 1.

The impact by EN on the morphology was most distinct at a deposition potential of -0.45 V vs. Ag/AgCl, as shown in the Fig. 2(c) and (d). Therefore the influence of EN concentration on Ag deposit morphology was further examined at this potential by varying the amount of EN, with the results presented in Fig. 3. With the EN concentration increasing from 0 to 40 mM, the size of bumps on the side branches gradually increased from around 170 to 600 nm (Fig. 3(a)–(c)). Finally, the dendrite became randomly distributed clusters at EN concentrations over 100 mM. The results further

supported the limiting reaction changing from mass transport to charge transport with EN addition.

The Ag catalysts fabricated with various EN concentrations were further used in the electrochemical reduction of CO<sub>2</sub> at -1.5 V vs. SCE for 1800 s, and the results are presented in Fig. 4. For Ag catalyst with no EN, the reduction current started at over 10 mA/cm<sup>2</sup>, then rapidly decreased with time (Fig. 4 (a)). The stabilized current was around 6.6 mA/cm<sup>2</sup>. For AgEN20 and AgEN40 catalysts, the reduction currents were reduced to around 3.5 mA/cm<sup>2</sup>. Higher EN concentrations during Ag electrodeposition resulted in a further decrease in reduction currents, to less than 1.5 mA/cm<sup>2</sup>, while the reduction was no more a strongly related function of EN concentration. The total reduction current was divided into partial currents for CO production (Fig. 4(b)) and H<sub>2</sub> production (Fig. 4(c)) using FE explained in a subsequent section. As clearly shown in these figures, the total current for AgENO was higher than for other catalysts, with most of the current corresponding to H<sub>2</sub> production. However, Ag catalysts fabricated in the presence of EN exhibited much lower H<sub>2</sub> partial currents than AgENO, and higher CO partial currents. For AgEN20 and AgEN40 in particular, the CO partial currents exhibited the highest value of 1.9 mA/cm<sup>2</sup>. This implied that Ag catalysts electrodeposited in the presence of EN were generally better catalysts for CO production than AgENO. Fig. 5 depicts the CO production activity of Ag catalysts in terms of FE and its normalized values with the mass of Ag deposits. As clearly shown in the figure, the very low FE of AgENO (10%) was greatly improved as EN concentration increased up to 40 mM (~60%). A further increase in EN concentration diminished the FE, producing a volcano plot according to EN concentration. This was also obvious in the mass activity; with increasing EN concentration, from 0 to 40 mM, the mass activity abruptly increased from 6.83 to 66.52%/mg<sub>Ag</sub> and then showed a tendency to decline, similar to the FE trend. These results strongly implied that EN made distinguishable changes in not only the apparent morphologies of the Ag deposits, but the intrinsic catalyst activity.

From the SEM images in Figs. 2 and 3, the addition of EN during electrodeposition might be expected to decrease the surface area of the Ag catalysts. This was further confirmed by LSV analysis in the potential range from -1.5 to 0.6 V vs. Ag/AgCl in N<sub>2</sub>-purged 0.1 M KOH, as presented in Fig. 6. In the LSV analysis, two characteristic peaks were observed at around -0.5 V (marked as peak 1) and 0.02 V (marked as peak 2). Although the kind of oxidation related to the peak 1 is still unclear, it is also definitely true that the peak is related to the oxidation of Ag, since the peak was not observed on Cu foil (the oxidation of bare Cu exhibited a slight peak at -0.3 V vs. Ag/AgCl). However, peak 2 corresponded to the oxidation of Ag to a monolayer of AgOH or Ag<sub>2</sub>O [45]. Using this known peak, the roughness factors (RFs) were calculated and compared. The RF values of Ag dendrites fabricated using AgENO, AgEN40, and AgEN400 solutions were 47.51, 20.98, and 9.65, respectively. The increase in EN concentrations from 0 to 40 and then 400 mM was shown to result in a significant decrement in RF values. This implied that EN addition had no positive impact on enlargement of the surface area, and had other stronger positive effects.

The influence of EN on the crystalline structure of the Ag catalysts was examined by XRD analysis. Fig. 7(a) shows the XRD patterns of AgENO and AgEN40 catalysts according to deposition

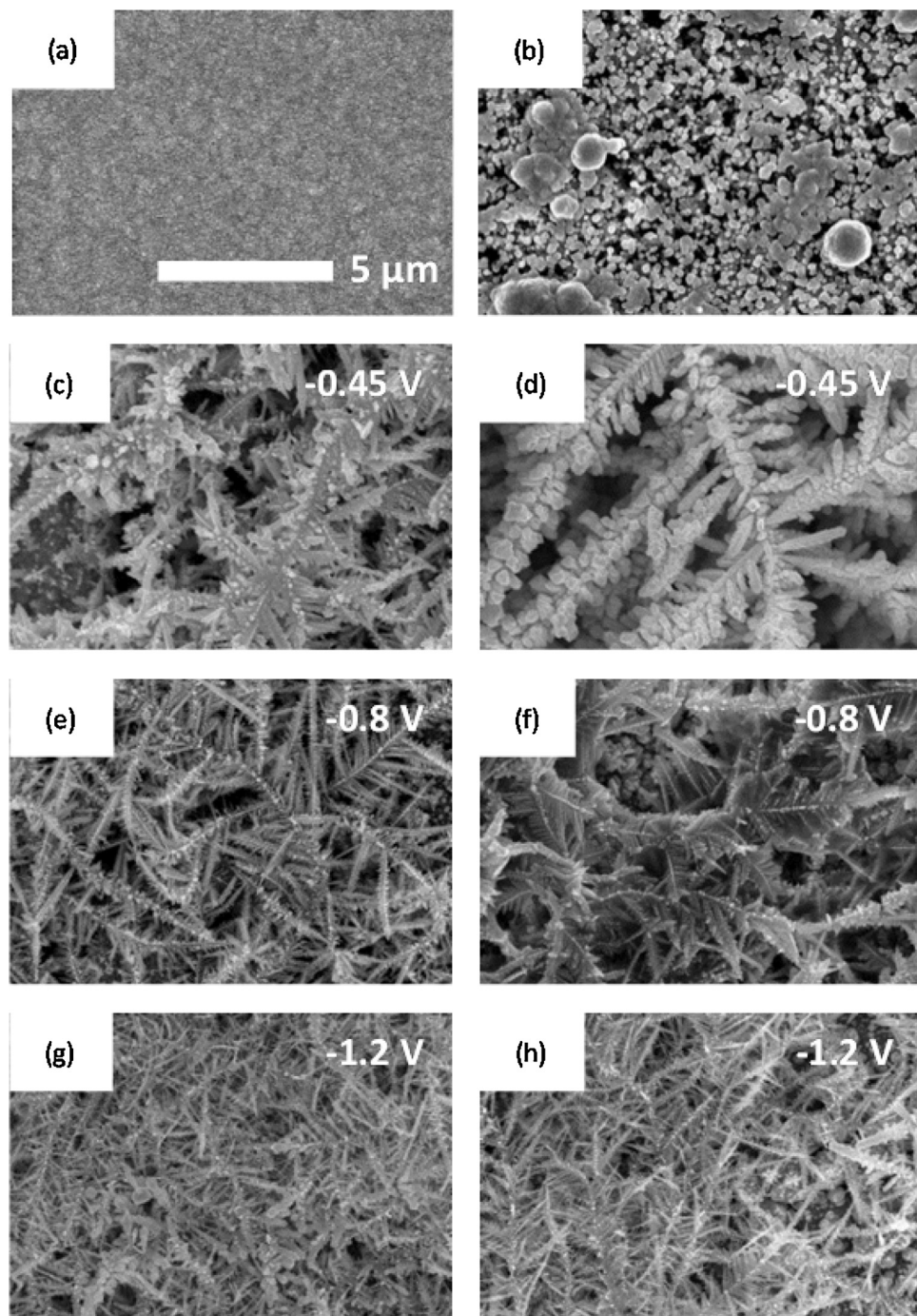


**Fig. 2.** FESEM images of (a) pristine Cu foil, (b) displaced Ag, and (c)–(h) electrodeposited Ag catalysts on displaced Ag from solutions (c, e, g) AgENO and (d, f, h) AgEN40. The deposition potentials were (c, d) –0.45 V, (e, f) –0.8 V, and (g, h) –1.2 V.

potentials of –0.45, –0.8, and –1.2 V vs. Ag/AgCl with a fixed deposition charge of  $1\text{ C}/\text{cm}^2$ . In contrast, Fig. 7(b) exhibits XRD patterns of Ag catalysts deposited at a fixed potential of –0.45 V vs. Ag/AgCl according to EN concentrations of AgENO, AgEN20, AgEN40, AgEN100, and AgEN400. The deposition charge was also fixed at  $1\text{ C}/\text{cm}^2$ . For all catalysts, the Ag peaks were observed at  $38.1^\circ$  (●),  $44.3^\circ$  (■),  $64.5^\circ$  (▲),  $77.4^\circ$  (★), and  $81.6^\circ$  (▼), which corresponded to crystal planes of Ag (111), Ag (200), Ag (220), Ag (311), and Ag (222), respectively. Three other peaks at  $43.2^\circ$  (○),  $50.4^\circ$  (□), and  $74.1^\circ$  (△) were related to Cu (111), Cu (200), and Cu (220), respectively. As shown in these figures, the relative intensities of all Ag peaks were roughly related to the deposition potential and EN

concentrations; generally, lower deposition potentials and higher EN concentrations resulted in higher Ag peaks. This was mainly due to the reaction being under the charge transport limitation through either lowering the deposition potential or inhibition of the deposition kinetics by added EN, as indicated in an earlier section.

As indicated by previous studies [22,23], the CO production efficiency was strongly affected by the crystalline structure, particularly the (110) plane. It would be helpful to quantitatively and directly measure the ratio of crystal orientation at the surface, but it is very difficult to precisely measure the surface orientation of 3-dimensional metal structure. Therefore, we adopted the intensity ratio of (220) and (111) peaks as a new descriptor for CO produc-

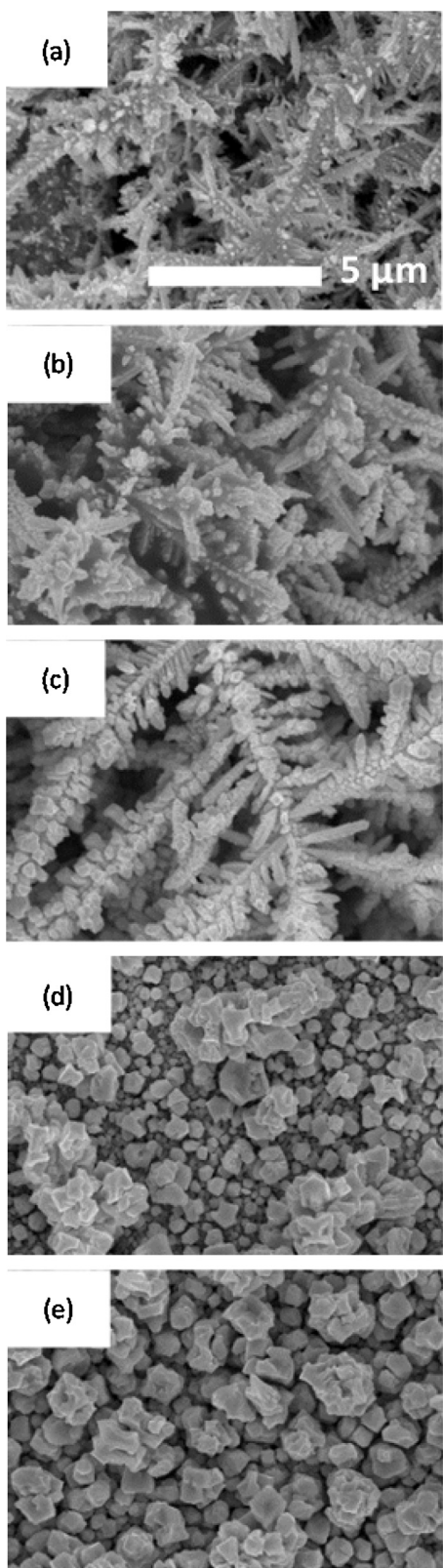


**Fig. 3.** FESEM images of Ag catalysts fabricated by electrodeposition at  $-0.45\text{ V}$  from solutions (a) AgEN0, (b) AgEN20, (c) AgEN40, (d) AgEN100, and (e) AgEN400.

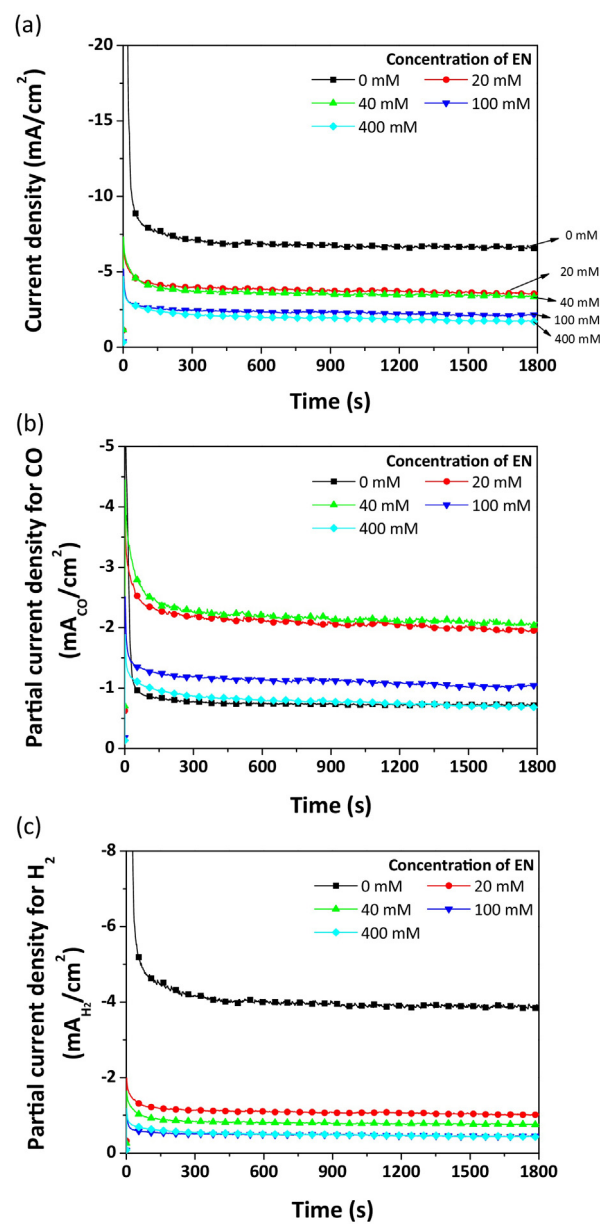


**Fig. 4.** (a) Total current density, (b) partial current density for CO, and (c) partial current density for H<sub>2</sub> during CO<sub>2</sub> reduction for 30 min at  $-1.5\text{ V}$  on Ag catalysts fabricated at  $-0.45\text{ V}$  with various EN concentrations. The current density was expressed by geometric area.

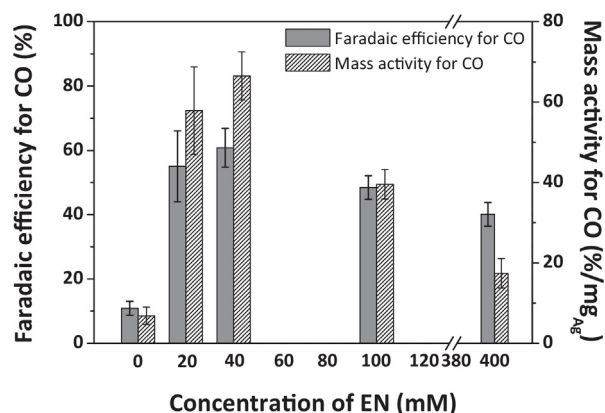


**Fig. 5.** FE for CO and its conversion to mass activity for Ag catalysts fabricated at  $-0.45\text{ V}$  with various EN concentrations.

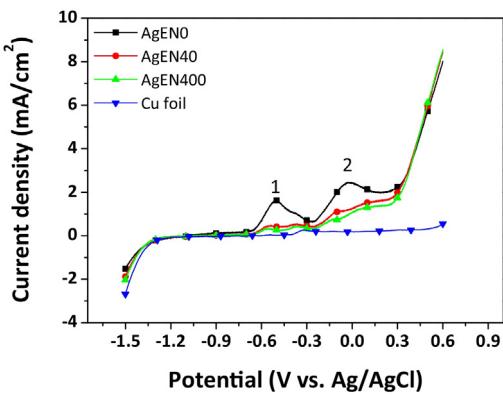


**Fig. 6.** CV of Ag catalysts fabricated at  $-0.45$  V in  $N_2$ -purged  $0.1$  M KOH. Potential range,  $-1.5$  to  $0.6$  V; scan rate,  $50$  mV/s.

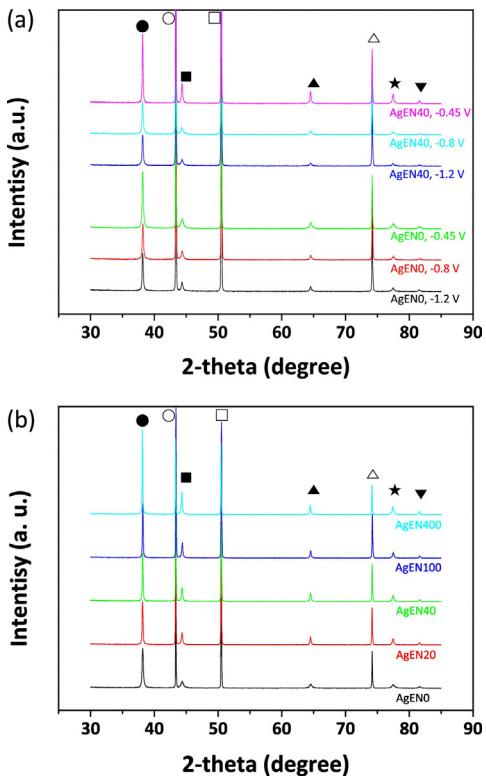


**Fig. 7.** XRD patterns of Ag catalyst (a) fabricated at various deposition potentials from AgENO and AgEN40 solution, and (b) fabricated at  $-0.45$  V using various electrodeposition solutions.

tion efficiency. Notably, the diffraction peak of Ag (110) was not observable in XRD patterns since the (110) reflection is forbidden in face centered cubic structures. However, the (110) structure was reasonably assumed to exist in an amount proportional to that of (220). Although it is impossible to quantitatively calculate the ratio of the surface crystal orientation from X-ray diffraction peaks, the relative amount of (220) surface can be estimated from (220)/(111) intensity ratio based on the growth mechanism of Ag dendrites.

The hierarchical Ag dendrite originates from the continuous fractal growth of Ag. The backbones grow from the substrate with preferred orientation (111) [50,51]. The hexagonal shape, whose surface consists of (111) and (100), forms at the edge of backbone, and branches then spread out from the backbone. This branching step continuously repeats and leads to the formation of hierarchical Ag dendrites. The angle between the growth directions of branch and sub-branch is between  $50$  and  $60$ ° because the branches grow

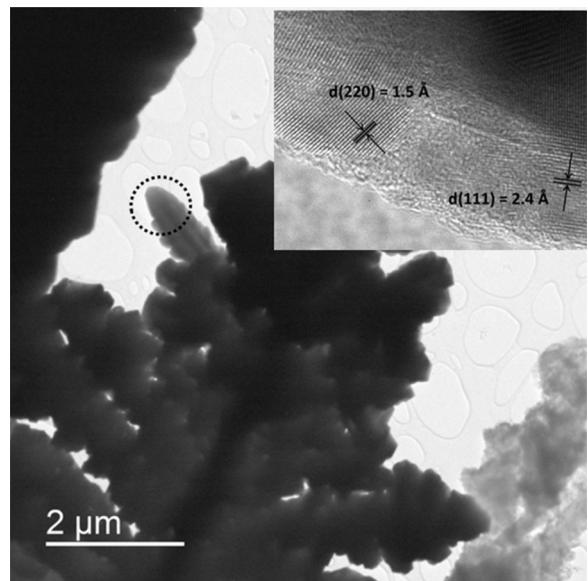


**Fig. 8.** Low and high (inset, circle point)-magnification transmission electron micrographs of Ag catalyst fabricated at  $-0.45$  V from AgEN40 solution.

with  $<100>$  direction from the edge of (111)-oriented backbone. Note that the angle between (111) and (100) crystal planes is  $55$ ° [50]. Ag dendrites in Figs. 2 and 3 also indicated that the difference in the growth direction was between  $50$  and  $60$ °, meaning the growth of Ag dendrite investigated in this study also follows same mechanism.

If Ag dendrites form via the same mechanism, the peak intensity ratio of (220) and (111) should be similar regardless of the size or density of Ag dendrites because Ag dendrite has a fractal geometry with polycrystalline [52,53]. Therefore, the increase in the (220)/(111) ratio means the additional growth of (220)-oriented Ag which was not related to the main dendrite formation. If (220)-oriented Ag strongly affects the branching step, the growth direction of dendrites would be changed. Interestingly, C. Gu et al. reported that (220)-oriented single crystal Ag can additionally grow at the edge of dendrites [54]. Since the additional growth of (220)-oriented Ag at the edge of dendrites can change Ag (220)/Ag (111) peak intensity ratio with sticking to the same growth mechanism for Ag dendrite, this additional growth of (220)-oriented Ag is responsible for an increase in Ag (220)/Ag (111) peak intensity ratio. Before we used the intensity ratio as a descriptor, we also confirmed the presence of the (220) structure on the surface by HRTEM analysis of the highest activity AgEN40 sample, as shown in Fig. 8.

The FEs of the product gases ( $H_2$  and CO) and the intensity ratio of Ag (220)/Ag (111) estimated from XRD analysis were correlated according to both the deposition potential (Fig. 9(a)) and EN concentration (Fig. 9(b)). For Ag catalysts deposited at  $-0.45$  V vs. Ag/AgCl (Fig. 9(a)), the addition of EN greatly improved the CO production efficiency, with a large reduction in  $H_2$  production, which was strongly attributed to the higher intensity ratio of (220)/(111) in AgEN40 compared with that of AgENO. As the deposition potential increased to  $-0.8$  V, the CO production efficiency of AgEN40 decreased slightly, simultaneous with the decrease in intensity ratio, while that of AgENO increased with an increase in intensity ratio. The trend was valid at a higher deposition potential of  $-1.2$  V for AgENO. However, AgEN40 deposition at  $-1.2$  V exhibited a similar intensity ratio to that at  $-0.8$  V, while the FE slightly increased. One more concern was that, at deposition potentials of  $-0.8$  and  $-1.2$  V, the intensity ratio for AgENO was higher than that of AgEN40, while the CO production efficiency of AgENO was

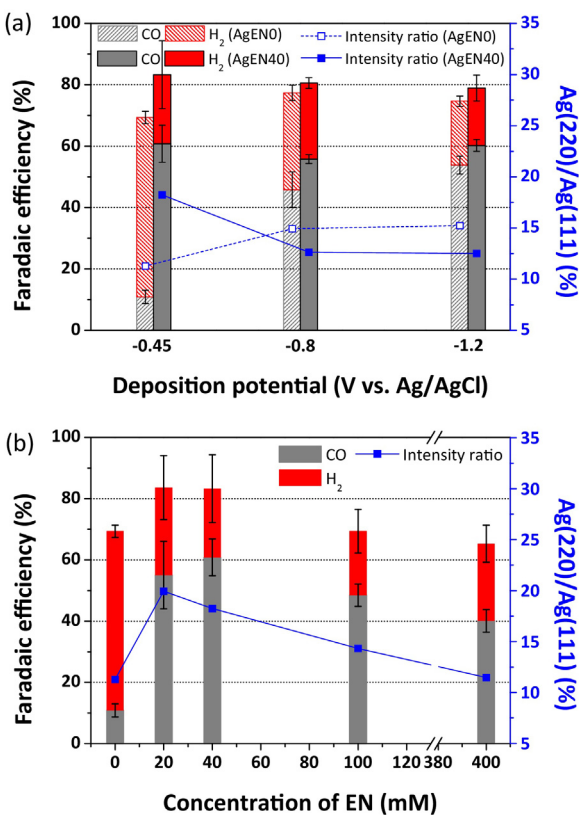


**Fig. 9.** Comparison of FEs of  $\text{CO}_2$  electrolysis at  $-1.5$  V with the (220)/(111) intensity ratio of Ag catalysts prepared by controlling (a) deposition potentials with fixed EN concentration and (b) EN concentrations with fixed deposition potential of  $-0.45$  V.

slightly lower than that of AgEN40. Leaving these deviations aside for now, the feasibility of the intensity ratio as a descriptor was further investigated according to the EN concentrations, as shown in Fig. 9(b). As already explained in Fig. 5, the CO production efficiencies are a strong function of EN concentrations, and exhibited the maximum FE of 60.81% at an EN concentration of 40 mM. The tendency of CO FE according to EN concentration strongly matched the tendency of the intensity ratio vs. EN concentration. This strongly supported the feasibility of using the (220)/(111) intensity ratio as an indicator for CO production efficiency, and the fact that the proper addition of EN during Ag electrodeposition enabled the fabrication of high activity catalysts for CO production by modulating the crystalline structures. However, some factors other than the crystalline structure were also involved in the CO production efficiency, which might be responsible for the deviations observed in Fig. 9(a).

To identify the other factors causing the mismatch between intensity ratio and CO production efficiency in Fig. 9(a), XPS analysis of various Ag catalysts was performed, and the resulting chemical shifts with respect to pure Ag [55] are presented at Fig. 10. Fig. 10(a) shows some representative XPS analyses of the Ag catalysts, while Fig. 10(b) and (c) show the chemical shifts of samples according to their deposition potentials and EN concentrations, respectively. Comparing Figs. 9(a) and 10(b) for the AgEN0 samples, the chemical shifts moving in a negative direction clearly has a positive effect on the CO production efficiency. It should also be noted that all AgEN40 samples in Fig. 10(b) have more negative chemical shift values than AgEN0 samples at each deposition potential. This was responsible for the higher CO FE of AgEN40 samples relative to AgEN0 samples in Fig. 9(a) (for samples at  $-0.8$  V and  $-1.2$  V), despite the lower (220)/(111) intensity ratios for AgEN40. Therefore, the electronic structure of the sample was another key factor affecting CO produc-

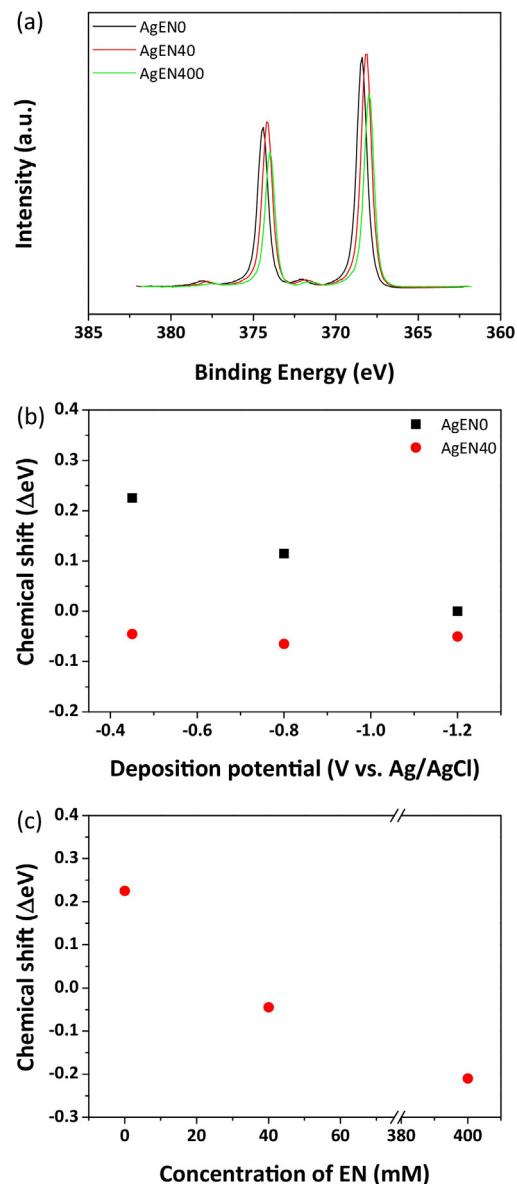


**Fig. 10.** (a) Some representative results of XPS spectra for Ag catalysts fabricated at  $-0.45$  V with various EN concentrations, and chemical shift of Ag 3d<sub>5/2</sub> obtained from XPS spectra by controlling (b) deposition potentials with fixed EN concentration and (c) EN concentrations with fixed deposition potential of  $-0.45$  V.

tion efficiency, and a compromise between the crystalline structure and electronic structure was necessary to precisely explain CO production efficiency behavior. As such, an easy interpretation is available in the comparison of Figs. 9(b) and 10(c); for AgEN0, a low intensity ratio and positive chemical shift were responsible for the poor CO production efficiency, while a relatively high intensity ratio and moderately negative chemical shifts resulted in the highest CO production efficiency. A similar explanation is possible for AgEN400 samples (low intensity ratio vs. highly negative chemical shift).

Shift in core-level binding energy toward negative direction might affect the binding strength of  $\text{COOH}^*$ , the most important reaction intermediate, on Ag catalyst surface. Rodriguez and Goodman have experimentally shown that a decrease in core-level binding energy caused by intermetallic electron transfer results in strong chemisorption of CO because of the high electron density of host metal that allows easy  $\pi$ -backdonation into adsorbed CO [56]. Their finding was theoretically supported by Hammer et al.

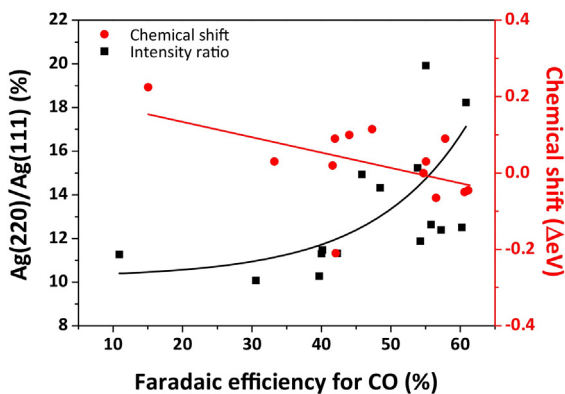


**Fig. 11.** A correlation of both the intensity ratio of Ag (220)/Ag (111) and the chemical shift of Ag catalysts with respect to the FE for CO.

who claimed that the normalized adsorption energy is roughly proportional to surface core level shift [57]. Considering the scaling relation [22], negative shift in core-level binding energy leads to the stabilization of  $\text{COOH}^*$  as well, thus increasing CO efficiency. There is also an argument that high electron density of catalyst itself, corresponding to the downshift of core level binding energy, leads to positive impact on  $\text{CO}_2$  reduction reaction in terms of reactivity channel [58]. Electron density on surface is fundamentally related to catalytic activity at electrochemically reducing potentials as it provides additional reactivity channels for  $\text{CO}_2$ .

For this generalization, we collected the intensity ratios and chemical shifts for all samples and correlated them with CO production efficiencies, regardless of the catalyst fabrication conditions, such as deposition potential, EN concentration, and deposition amounts. As clearly shown in Fig. 11, despite some deviations, the two parameters successfully indicate the directions for better CO production catalysts; higher (220)/(111) intensity ratios and more negative chemical shifts result in better CO production efficiencies. Moreover, the electrodeposition of Ag in the presence of the appropriate concentration of EN enables both parameters to be controlled easily and simultaneously. The mechanisms for modification of the crystalline and electronic structures of Ag deposits by EN remain to be interpreted by future studies aiming to develop better additives for this purpose, for which the clues can be found in literature on the adsorption of additives and their subsequent actions in controlling the growth and shape of metal deposits [59–63].

#### 4. Conclusions

In this study, dendrite-type Ag catalysts for the electrochemical reduction of  $\text{CO}_2$  were prepared via electrodeposition from an ammonia-based Ag deposition solution containing EN as an additive. The addition of EN during Ag electrodeposition changed the diffraction peak intensity ratio of the (111) and (220) planes, as well as their electronic states. The CO production efficiencies of the prepared Ag catalysts were found to be a function of both the crystalline and electronic structures of the Ag deposits, i.e., the higher the (220)/(111) intensity ratio and more negative the chemical shifts, the better the resultant CO production efficiency. This relationship suggested a guideline for the design of CO production catalysts in the electrochemical conversion of  $\text{CO}_2$ .

#### Acknowledgments

This work was supported by a grant from the Korea CCS R&D Center (KCRC) funded by the Korea government (NRF-2014M1A8A1049349).

#### References

- [1] Y. Hori, K. Kikuchi, S. Suzuki, *Chem. Lett.* (1985) 1695–1698.
- [2] Y. Hori, H. Wakebe, T. Tsukamoto, O. Koga, *Electrochim. Acta* 39 (1994) 1833–1839.
- [3] H. Yano, F. Shirai, M. Nakayama, K. Ogura, *J. Electroanal. Chem.* 533 (2002) 113–118.
- [4] M. Gattrell, N. Gupta, A. Co, *Energy Convers. Manage.* 48 (2007) 1255–1265.
- [5] B.A. Rosen, A. Salehi-Khojin, M.R. Thorson, W. Zhu, D.T. Whipple, P.J. Kenis, R.I. Masel, *Science* 334 (2011) 643–644.
- [6] J.P. Jones, G. Prakash, G.A. Olah, *Isr. J. Chem.* 54 (2014) 1451–1466.
- [7] J. Durst, A. Rudnev, A. Dutta, Y.C. Fu, J. Herranz, V. Kaliginedi, A. Kuzume, A.A. Permyakova, Y. Paratcha, P. Broekmann, T.J. Schmidt, *Chimia* 69 (2015) 769–776.
- [8] Y. Hori, *Electrochemical  $\text{CO}_2$  reduction on metal electrodes*, in: C. Vayenas, R. White, M. Gamboa-Aldeco (Eds.), *Modern aspects of electrochemistry*, Springer, New York, 2008, pp. 89–189.
- [9] Y. Zhang, G. Jacobs, D.E. Sparks, M.E. Dry, B.H. Davis, *Catal. Today* 71 (2002) 411–418.
- [10] Y. Chen, C.W. Li, M.W. Kanan, *J. Am. Chem. Soc.* 134 (2012) 19969–19972.
- [11] D. Kim, J. Resasco, Y. Yu, A.M. Asiri, P. Yang, *Nat. Commun.* 5 (2014) 4948.
- [12] Q. Lu, J. Rosen, Y. Zhou, G.S. Hutchings, Y.C. Kimmel, J.G. Chen, F. Jiao, *Nat. Commun.* 5 (2014) 3242.
- [13] J. Rosen, G.S. Hutchings, Q. Lu, R.V. Forest, A. Moore, F. Jiao, *ACS Catal.* 5 (2015) 4586–4591.
- [14] D. Gao, H. Zhou, J. Wang, S. Miao, F. Yang, G. Wang, J. Wang, X. Bao, *J. Am. Chem. Soc.* 137 (2015) 4288–4291.
- [15] C. Delacourt, P.L. Ridgway, J. Newman, *J. Electrochem. Soc.* 157 (2010) B1902–B1910.
- [16] T. Hatsukade, K.P. Kuhl, E.R. Cave, D.N. Abram, T.F. Jaramillo, *PCCP* 16 (2014) 13814–13819.
- [17] Y.-C. Hsieh, S.D. Senanayake, Y. Zhang, W. Xu, D.E. Polyansky, *ACS Catal.* 5 (2015) 5349–5356.
- [18] J. Rosen, G.S. Hutchings, Q. Lu, S. Rivera, Y. Zhou, D.G. Vlachos, F. Jiao, *ACS Catal.* 5 (2015) 4293–4299.
- [19] A. Salehi-Khojin, H.R.M. Jhong, B.A. Rosen, W. Zhu, S. Ma, P.J. Kenis, R.I. Masel, *J. Phys. Chem. C* 117 (2013) 1627–1632.
- [20] C. Kim, H.S. Jeon, T. Eom, M.S. Jee, H. Kim, C.M. Friend, B.K. Min, Y.J. Hwang, *J. Am. Chem. Soc.* 137 (2015) 13844–13850.
- [21] A.A. Peterson, J.K. Nørskov, *J. Phys. Chem. Lett.* 3 (2012) 251–258.
- [22] S. Back, M.S. Yeom, Y. Jung, *ACS Catal.* 5 (2015) 5089–5096.
- [23] N. Hoshi, M. Kato, Y. Hori, *J. Electroanal. Chem.* 440 (1997) 283–286.
- [24] S.H. Ahn, O.J. Kwon, S.K. Kim, I. Choi, J.J. Kim, *Int. J. Hydrogen Energy* 35 (2010) 13309–13316.
- [25] S.H. Ahn, S.J. Hwang, S.J. Yoo, I. Choi, H.J. Kim, J.H. Jang, S.W. Nam, T.H. Lim, T. Lim, S.K. Kim, *J. Mater. Chem.* 22 (2012) 15153–15159.
- [26] S. Sen, D. Liu, G.T.R. Palmore, *ACS Catal.* 4 (2014) 3091–3095.
- [27] B.S. Lee, S.H. Ahn, H.Y. Park, I. Choi, S.J. Yoo, H.J. Kim, D. Henkensmeier, J.Y. Kim, S. Park, S.W. Nam, *Appl. Catal. B: Environ.* 179 (2015) 285–291.
- [28] D.H. Won, C.H. Choi, J. Chung, M.W. Chung, E.H. Kim, S.I. Woo, *ChemSusChem* 8 (2015) 3092–3098.
- [29] J.F. Xie, Y.X. Huang, H.Q. Yu, *Front. Environ. Sci. Eng.* 9 (2015) 861–866.
- [30] J. Choi, M.J. Kim, S.H. Ahn, I. Choi, J.H. Jang, Y.S. Ham, J.J. Kim, S.K. Kim, *Chem. Eng. J.* 299 (2016) 37–44.
- [31] S.H. Ahn, S.J. Yoo, H.J. Kim, D. Henkensmeier, S.W. Nam, S.-K. Kim, J.H. Jang, *Appl. Catal. B: Environ.* 180 (2016) 674–679.
- [32] J.E. Lim, U. Lee, S.H. Ahn, E. Cho, H.J. Kim, J.H. Jang, H. Son, S.K. Kim, *Appl. Catal. B: Environ.* 165 (2015) 495–502.
- [33] J.Y. Kim, J. Choi, H.Y. Kim, E. Hwang, H.J. Kim, S.H. Ahn, S.-K. Kim, *Appl. Surf. Sci.* 359 (2015) 227–235.
- [34] Z.B. Lin, J.H. Tian, B.G. Xie, Y.A. Tang, J.J. Sun, G.N. Chen, B. Ren, B.W. Mao, Z.Q. Tian, *J. Phys. Chem. C* 113 (2009) 9224–9229.
- [35] Z.B. Lin, B.G. Xie, J.H. Tian, Y.A. Tang, J.J. Sun, G.N. Chen, B. Ren, B.W. Mao, Z.Q. Tian, *J. Electroanal. Chem.* 636 (2009) 74–79.
- [36] T. Osaka, N. Yamachika, M. Yoshino, M. Hasegawa, Y. Negishi, Y. Okinaka, *Electrochim. Solid-State Lett.* 12 (2009) D15–D17.
- [37] J.E. Ferguson, C. Boldt, A.D. Redish, *Sens. Actuators A Phys.* 156 (2009) 388–393.
- [38] G. Zarkadas, A. Stergiou, G. Papanastasiou, *Electrochim. Acta* 50 (2005) 5022–5031.
- [39] S.H. Hong, S.H. Ahn, I. Choi, S.G. Pyo, H.J. Kim, J.H. Jang, S.K. Kim, *Appl. Surf. Sci.* 307 (2014) 146–152.
- [40] S.H. Hong, S.H. Ahn, I. Choi, J.Y. Kim, H.Y. Kim, H.J. Kim, J.H. Jang, H. Kim, S.K. Kim, *Appl. Surf. Sci.* 349 (2015) 629–635.
- [41] S. Kaniyankandy, J. Nuwad, C. Thinaharan, G. Dey, C. Pillai, *Nanotechnology* 18 (2007) 125610.
- [42] T. Iida, M. Yoshino, J. Sasano, I. Matsuda, T. Osaka, *J. Surface Finishing Soc. Japan* 55 (2004) 962–963.
- [43] M.J. Kim, H.J. Lee, S.H. Yong, O.J. Kwon, S.-K. Kim, J.J. Kim, *J. Electrochem. Soc.* 159 (2012) D253–D259.
- [44] M.J. Kim, T. Lim, K.J. Park, O.J. Kwon, S.K. Kim, J.J. Kim, *J. Electrochem. Soc.* 159 (2012) D544–D548.
- [45] J.G. Becerra, R. Salvarezza, A. Arvia, *Electrochim. Acta* 33 (1988) 1431–1437.
- [46] W. Zhu, R. Michalsky, O.n. Metin, H. Lv, S. Guo, C.J. Wright, X. Sun, A.A. Peterson, S. Sun, *J. Am. Chem. Soc.* 135 (2013) 16833–16836.

[47] D. Reyter, D. Bélanger, L. Roué, *Electrochim. Acta* 53 (2008) 5977–5984.

[48] G. Lacconi, A. Gioda, V. Macagno, *Electrochim. Acta* 30 (1985) 211–215.

[49] G. De Oliveira, L. Barbosa, R. Broggi, I. Carlos, *J. Electroanal. Chem.* 578 (2005) 151–158.

[50] X. Wen, Y.T. Xie, W.C. Mak, K.Y. Cheung, X.Y. Li, R. Renneberg, S. Yang, *Langmuir* 22 (2006) 4836–4842.

[51] J. Fang, H. You, C. Zhu, P. Kong, M. Shi, X. Song, B. Ding, *Chem. Phys. Lett.* 439 (2007) 204–208.

[52] X. Qin, Z. Miao, Y. Fang, D. Zhang, J. Ma, L. Zhang, Q. Chen, X. Shao, *Langmuir* 28 (2012) 5218–5226.

[53] W. Ye, Y. Chen, F. Zhou, C. Wang, Y. Li, *J. Mater. Chem.* 22 (2012) 18327–18334.

[54] C. Gu, T.Y. Zhang, *Langmuir* 24 (2008) 12010–12016.

[55] G. Johansson, J. Hedman, A. Berndtsson, M. Klasson, R. Nilsson, *J. Electron. Spectrosc. Relat. Phenom.* 2 (1973) 295–317.

[56] J.A. Rodriguez, D.W. Goodman, *Science* 257 (1992) 897–903.

[57] B. Hammer, Y. Morikawa, J.K. Nørskov, *Phys. Rev. Lett.* 76 (1996) 2141.

[58] B. Patrick Sullivan, *Platinum Met. Rev.* 33 (1989) 2–9.

[59] F. Lallemand, L. Ricq, M. Wery, P. Berçot, J. Pagetti, *Surf. Coat. Technol.* 179 (2004) 314–323.

[60] R. Sekar, C. Eagamai, S. Jayakrishnan, *J. Appl. Electrochem.* 40 (2010) 49–57.

[61] R. Manu, S. Jayakrishnan, *Bull. Mater. Sci.* 34 (2011) 347–356.

[62] K. Nayana, T. Venkatesha, *J. Electroanal. Chem.* 663 (2011) 98–107.

[63] A. Liu, X. Ren, J. Zhang, G. Yuan, P. Yang, J. Zhang, M. An, *New J. Chem.* 39 (2015) 2409–2412.